IEEE Access
Multidisciplinary | Rapid Review | Open Access Journal

Received March 8, 2020, accepted March 25, 2020, date of publication March 30, 2020, date of current version April 16, 2020.

Digital Object Identifier 10.1109/ACCESS.2020.2984010

A Compact Vivaldi Antenna With Artificial Material Lens and Sidelobe Suppressor for GPR Applications

HOUYUAN CHENG[1], HELIN YANG[1], YUJUN LI[1], AND YIQUN CHEN[2]
[1]College of Physical Science and Technology, Central China Normal University, Wuhan 430079, China
[2]Key Laboratory of Exploration Technologies for Oil and Gas Resources, Ministry of Education, Yangtze University, JingZhou 434000, China

Corresponding author: Helin Yang (emyang@mail.ccnu.edu.cn)

This work was supported in part by the National Natural Science Foundation of China under Grant 41774116, and in part by the Fundamental Research Funds for the Central Universities, China, under Grant CCNU19CG013 and Grant CCNU18JCXK02.

ABSTRACT A novel compact Vivaldi Antenna (CVA) for short-pulse ground penetrating radar (GPR) systems is presented. Artificial materials lens (AML) and sidelobe suppressor (SSR) are loaded to improve GPR Antenna's radiation capability in the aperture and the flanks of the CVA. The simulation and experimental results indicate that the proposed CVA has a −10 dB impedance bandwidth of 100% (0.7-2.1 GHz) and a −3 dB gain bandwidth of 70.9% (1.0-2.1 GHz). Within the operating bandwidth of the CVA, AML primarily enhances the CVA's high-frequency gain (1.4-2.1GHz), while the SSR primarily enhances the CVA's low-frequency gain (0.7-1.4 GHz). Moreover, the CVA loaded with two kinds of artificial materials (AMs) has an average gain of 1 dB and 2 dB in the low-frequency and high-frequency parts, respectively. In addition, the transmission response with small ringing in time domain makes the proposed CVA suitable for short-pulse GPR systems. AML and SSR effectively enhance the gain of the CVA with a compact and space-saving loading method, which provides a new idea to enhance the gain of the CVA by artificial material.

INDEX TERMS Vivaldi antenna, artificial material, low-frequency gain enhancement.

I. INTRODUCTION

Benefiting from its good performance, Vivaldi antennas have been widely used in wireless communication systems, such as satellite communications, microwave imaging and ground penetrating radar (GPR) [1], [2]. To survey the soil composition under the ground, the GPR needs to emit high-power pulses to the ground. To make the signal transmit deeper and to make its resolution higher, GPR's antennas are required to have a lower operating band, ultra-wideband and high gain [3]. GPR's antennas come in different types in different survey environments. Among the common GPR's antenna types such as dipole antennas [4], bowtie antennas [5], [6] and Vivaldi antennas [7], [8], Vivaldi antennas are the most common and widely used owing to their ultra-wideband, high directivity, and low cross-polarization.

In order to enhance the gain of the antenna, many methods have been proposed by researchers. Among them, antenna arrays [9], etching grooves [10] and dielectric lenses [11] have become widely used technologies. The antenna arrays can effectively enhance the gain, but the coupling and power distribution need to be considered, which makes it complicated to design. Slotting on the antenna can lower the operating frequency of the antenna and enhance the gain, but this will degrade the directivity of the antenna. Loading a high dielectric constant lens can stably enhance the gain of the antenna, but its improvement is limited [12]. Besides several common methods described above, method of loading artificial materials (AMs) on antennas had also been noticed and extensively explored by researchers since AMs have been proposed. There are many typical AMs applied to the antenna, including zero-index materials, frequency selective surfaces, gradient metasurface, and photonic crystals. In [13], the authors designed a multi-layer S-type resonator with zero index to enhance the gain of the antenna. In addition, a multi-layer coupled FSS had been proposed in [14] to enhance the gain of the antenna. In [15], a multi-layered gradient super-surface was used as a lens and loaded in front of the aperture of the antenna, which also enhance the gain of the antenna significantly in a wide frequency. The methods mentioned

The associate editor coordinating the review of this manuscript and approving it for publication was Ildiko Peter.

TABLE 1. Design parameters of the CVAs and AMs (unit:mm).

x_1	x_2	x_3	x_4	y_1	y_2
240	46	60	121	240	70
y_3	y_4	w_0	w_1	w_2	$w_3 = w_6$
160	23	13.6	12	5	2
w_4	w_5	$w_7 = w_9$	w_8	l_0	l_1
11	10	1	9.5	13	1
l_2	l_3	l_4	l_5	r	D
3	2	11	2.5	24	36

above can effectively enhance the gain of the antenna, but all have a ommon disadvantage that the design of the multilayer structure increases the size of the antenna and complicates the fabrication [16]. Moreover, photonic crystals, as a kind of all-media artificial material, have good effects on gian enhancement, but they are expensive and difficult to manufacture [17]. Finally, it is worth noting that the working bandwidth of AMs becomes narrower and the gain enhancement becomes worse as the operating frequency decreases, which makes it limited in GPR's applications [18], [19]. To overcome these limitations and enhance the gain of the antenna over the entire operating band, in this paper, we load AML and SSR simultaneously in the aperture and flanks of the antenna. Besides, the proposed antenna structure is compact and simple, which makes it widely applicable to GPR.

This manuscript is organized as follows. In Section II, We give a 2D geometry of the original CVA and improved CVA (CVAs), as well as some basic parameters of the CVAs, including simulated and measured S11 parameters, antenna gain and radiation patterns. In Section III, Some characteristicFig. such as transmission properties, effective electromagnetic parameters and electric field distribution are studied to present the coupling mechanism between AMs and the original CVA. Finally Section IV concludes this paper.

II. AMs-BASED CVA DESIGN AND RESULTS

In this section, with simulation and experimental results shown to compare their performance, the original and AMs-based CVA design are presented.

A. ANTENNA DESIGN

The planar model of the original CVA is shown in Fig. 1(a). FR-4, whose thickness is h = 1.52 mm as well as relative permittivity and tangent loss are $\varepsilon_r = 4.3$ and $\delta = 0.025$, is chosen as the dielectric substrate. CVA's coated metal

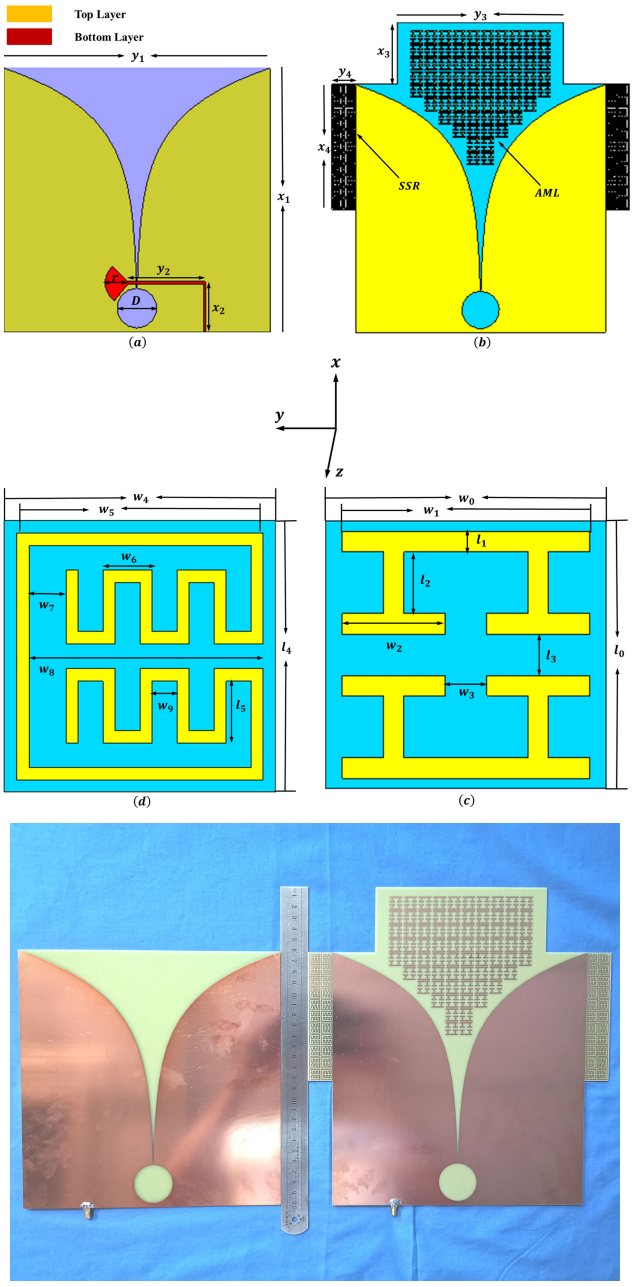

FIGURE 1. (a) Schematic diagram of the CVA. (b) Schematic diagram of CVA with AMs. (c) Schematic diagram of AML, (d) Schematic diagram of SSR and (e) test antennas board.

consists of two parts - the top layer and the bottom layer. The top layer is the main radiating metal. The aperture profile of the CVA is plotted by an exponential function, i.e. $y = e^{0.024x}(0 \leq x \leq 200)$, and the bottommost spacing of the aperture trenches is 0.5 mm connected to the hollowed-out circular holes. The feed line on the bottom layer consists of two segments with a width of 2 mm and the feed is a fan with an angle of 100 degrees. The metal patches of CVA are copper with thickness of 0.035 mm. The plane model diagram of the proposed antenna is given in Fig. 1(b). The proposed antenna is a CVA loaded with two types of AMs,

TABLE 2. Gain improvement and half power beam width.

Frequency (GHz)	CVA without AMs E-Plane (degree)	CVA without AMs H-Plane (degree)	CVA with AMs E-Plane (degree)	CVA with AMs H-Plane (degree)	Antenna gain improvement (dB)
0.7 GHz	68.6	160.6	63.8	145.9	1
1.4 GHz	51.9	106.9	46.7	76.6	1.63
2.1 GHz	49.3	62.0	39.4	45.6	1.89

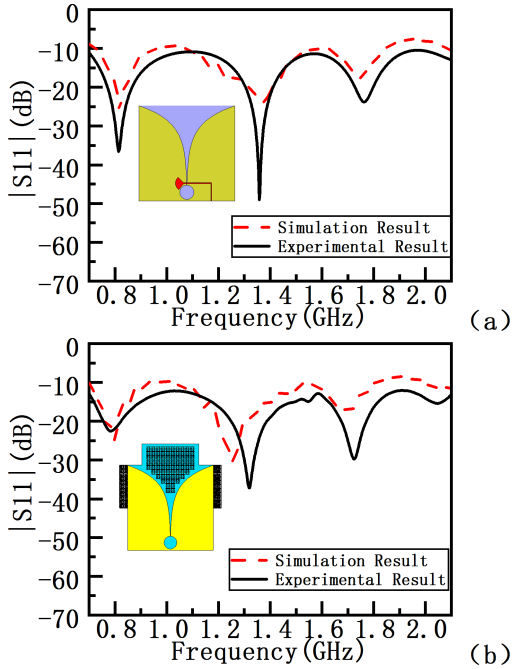

FIGURE 2. (a) |S11| (in dB) of the CVA. Inset: photograph of the CVA. (b) |S11| (in dB) of the CVA with AMs. Inset: photograph of the CVA with AMs.

where AML is loaded at the front end of the antenna and SSR is loaded on the side of the antenna. The geometry of AML and SSR are shown in Fig. 1(c) and (d), respectively. All the detailed dimensions of the antennas and AMs are shown in Table 1. Finally, the positions of all models refer to the same coordinate system, which can be seen in Fig.1.

B. SIMULATION AND EXPERIMENTAL RESULTS OF THE CVAs

In this sub-section, we analyzed some important performances of the CVAs, including the S parameters, radiation gain, radiation patterns and transmission.

1) S PARAMETERS

The S11 parameters for CVA with and without AMs are shown in Fig. 2 (a) and (b). We can find that the reflection coefficients of CVA with and without AMs are below −10 dB in the working band. It can be seen that the loading

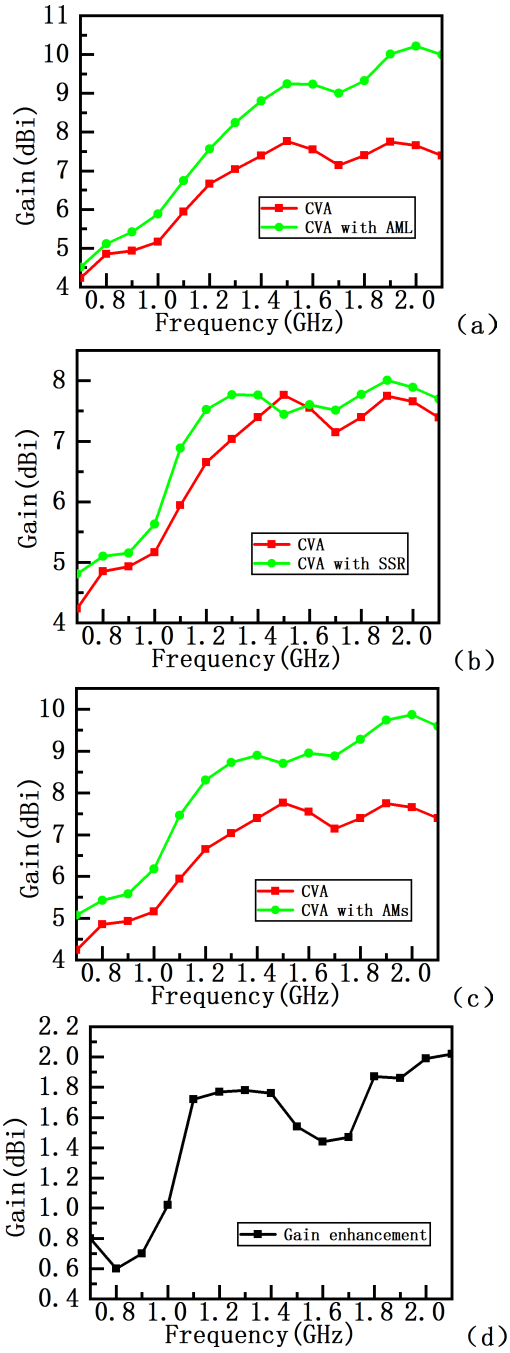

FIGURE 3. (a) Simulated gain of CVA with AML. (b) Simulated gain of CVA with SSR. (c) Simulated gain of CVA with AMs. (d) measured gain enhancement of CVA and CVA with AMs.

of AMs has no effect on the impedance bandwidth of the CVA. In addition, the simulation results are in good agreement with the experimental results, which also proves the feasibility of the model. Finally, the S11 parameter of the proposed antenna has a relative bandwidth of 100% (0.7-2.1 GHz), which is consistent with that of CVA. The mechanism of good impedance match between AMs and antennas will be demonstrated and explained in detail in the next section.

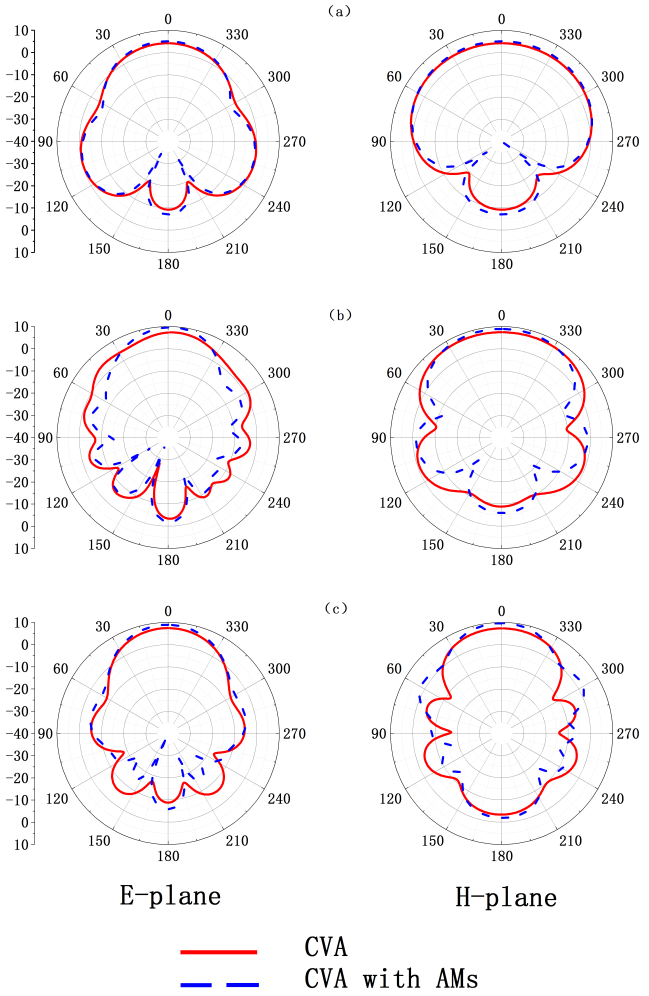

FIGURE 4. Simulated radiation patterns of CVAs. (a) (b) and (c) are E-plane and H-plane at 0.7 GHz, 1.4 GHz and 2.1 GHz.

2) RADIATION GAIN

Fig.3 (a) and (b) illustrates the simulated radiation gain of CVAs from 0.7 to 2.1 GHz, respectively. It can be found that AML enhances the CVA's high-frequency (1.4-2.1 GHz) gain primarily. while the SSR primarily enhances the CVA's low-frequency gain (0.7-1.4 GHz). In Fig. 3(c),compared to the original antenna, the CVA with AMs stably enhance the gain over the entire operating band. The gain is enhanced by an average of 1 dB at low frequencies (0.7-1.4 GHz) and by an average of 2 dBat high frequencies (1.4-2.1 GHz). The −3 dB gain bandwidth of the proposed antenna is 70.9% (1.2-2.1 GHz). The experimental gain enhancements of CVA and CVA with AMs are shown in Fig. 3 (d). The next section will show how AMs affect the gain of the antenna.

3) RADIATION PATTERNS

The simulation and experimental E-planes and H-planes are shown in Fig. 4 and 5, respectively. In these figures, the solid red line and the blue dashed line are used to indicate the patterns of the CVA with and without AMs, respectively.

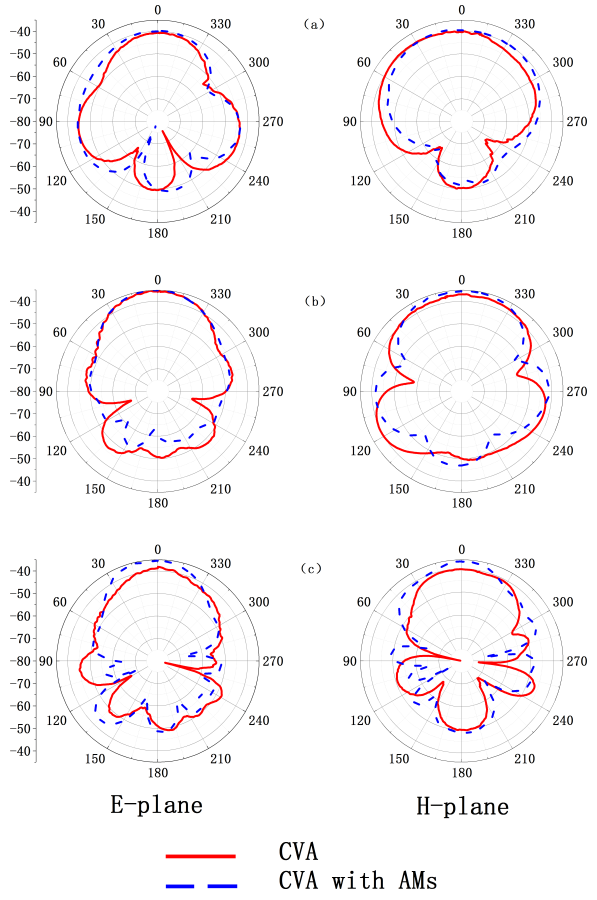

FIGURE 5. Experimental radiation patterns of CVAs. (a) (b) and (c) are E-plane and H-plane at 0.7 GHz, 1.4 GHz and 2.1 GHz.

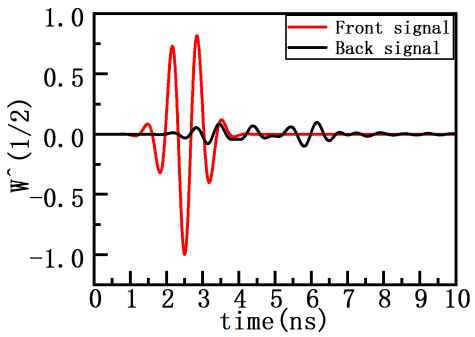

FIGURE 6. The comparison between the front signal and back signal.

In the operating frequency band, patterns are depicted at three typical frequency points which are 0.7 GHz, 1.4 GHz and 2.1 GHz. First, we can see that the radiation of CVA with AMs is improved in the end-fire direction, which is the most obvious at 2.1 GHz. In Fig. 4, with the increase of frequency, the radiation direction of the antenna is concentrated more, which is consistent with the gain curve mentioned above. In Fig. 5, the experimental radiation patterns of the antenna are given. The results of the simulation are consistent with the results of the experiment.

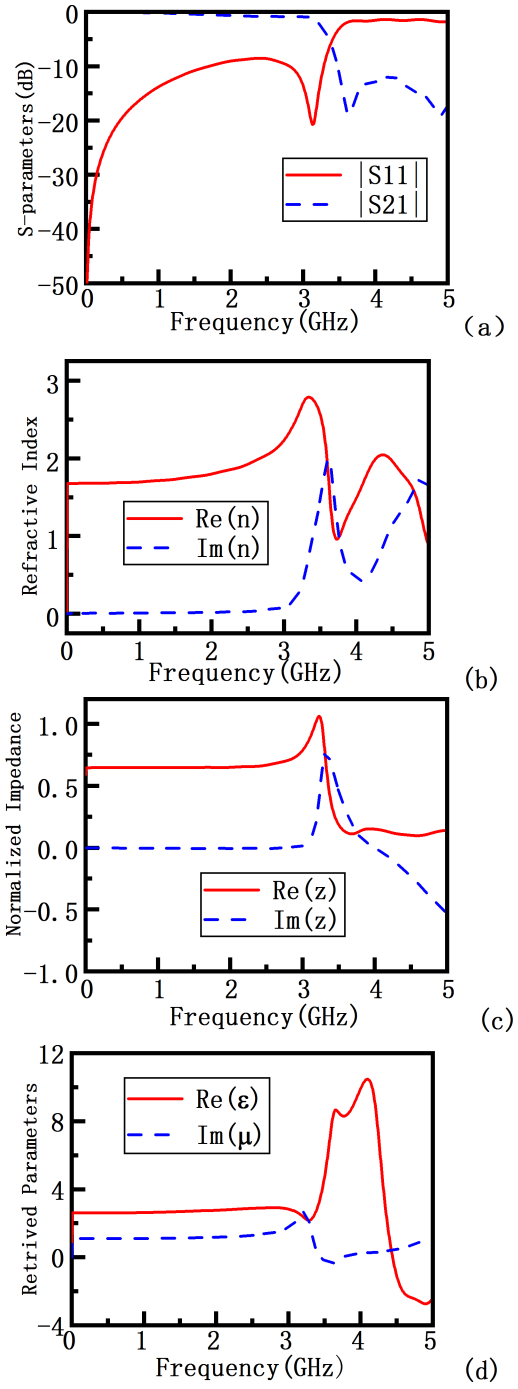

FIGURE 7. (a) Simulated S parameters, (b) retrieved refractive index, (c) retrieved impedance, (d) retrieved relative permittivity and permeability.

Table 2 illustrates the antenna gain improvement and half-power beam width of the E-planes and H-planes. In order to show the radiation performance of the antenna more specifically, we still utilized the three typical frequency points mentioned above as the research frequency. It can be foud that the half-power beam width of the CVAS's E-plane decreases with increase of the frequency. Besides, compared with the original antenna, the half-power beam width of the E-plane of

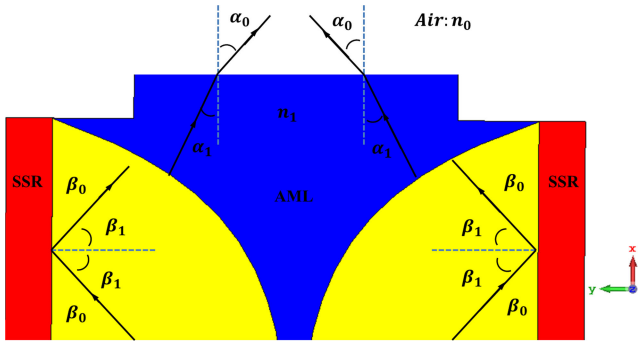

FIGURE 8. The refraction and reflection phenomenon of electromagnetic wave from the AMs to air.

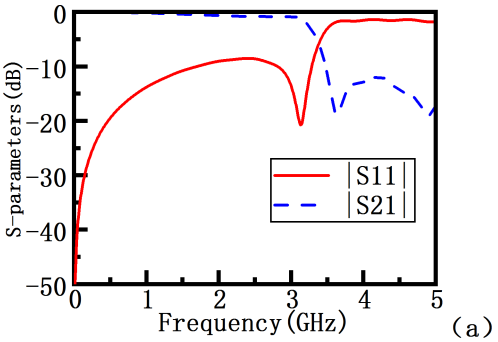

FIGURE 9. Simulated S parameters of SSR.

the proposed antenna is reduced. Among them, the proposed antenna has a minimum half-power beam of 39.4 degrees at 2.1 GHz. This means that when the antenna is loaded with AMs, the energy gets more concentrated.

Furthermore, the operating frequency band, gain enhancement mechanism and other properties of the proposed antenna are compared to existing works in Table 3. As can be seen from Table 3, the proposed antenna has general impedance bandwidth and gain bandwidth properties, but it can effectively improve the antenna's low frequency gain with a simple manufacturing, which can be well distinguished from other antennas.

4) TRANSMISSION RESPONSE

In order to verify and demonstrate that the proposed antenna is well suitable for GPR systems, we analyze the transmission response of the antenna in the time domain. As shown in Fig. 6, the front and back radiation signals of the proposed antenna are extracted from the CST. The ratio of the front radiation signal to the back radiation signal is approximately 10:1. Moreover, a small late-time ringing demonstates that the proposed antenna can be applied to GPRs.

III. COUPLING MECHANISM FOR THE PROPOSED CVAs

Analyzing electromagnetic properties of the proposed AMs, we can reveal the coupling mechanism between the CVA and the AMs. The unit cell of the AML is shown in Fig. 1(c). In the reference coordinate system of Fig. 1, boundary conditions are set follow. The face perpendicular to the y-axis is set as a perfect electric wall, the face perpendicular to the z-axis is set

TABLE 3. Performance comparison of the proposed CVA and similar published work.

	-10 dB Impedance bandwidth	-3 dB gain bandwidth	Manufacturing process	Minimum operating frequency gain enhancement	Gain enhancement mechanism
This paper	100% 0.7-2.1 GHz	70.9% 1-2.1 GHz	Single layer, simple	1 dB	Non-resonant lens and sidelobe suppressor
[18]	104% 6-19 GHz	86.8% 7.5-19 GHz	Single layer, simple	About 0.6 dB	Non-resonant lens
[15]	56.7% 6.7-12 GHz	61.4% 7-13.2 GHz	Multi-layer, complex	About 4 dB	Gradient metasurface lens
[21]	144.8% 2-12.5 GHz	122.5% 3-12.5 GHz	Single layer, simple	About 0.1 dB	Dielectric lens
[13]	142.8% 2-12 GHz	62.9% 6-11.5 GHz	Multi-layer, complex	About 0.2 dB	Zero-Index Metamaterial

as a perfect magnetic wall, and the face perpendicular to the x-axis is set as an open boundary. Such a setup simulates the process of electromagnetic waves passing through the AML along the x-axis, so the simulated electromagnetic parameters can characterize the electromagnetic properties of the AML.

The simulated reflection coefficient and transmission coefficient are shown in Fig.7(a). it can be seen that the magnitude of reflection coefficients (|S11|) in dB are less than -10 dB and the transmission coefficients (|S21|) are about 0 dB over 0.7-2.1 GHz. It means that most of the electromagnetic waves in this band can pass through the AML with little loss, which is the most basic characteristic of the lens. Besides, other electromagnetic parameters of the material, such as refractive index, impedance, relative permittivity and permeability, are derived from the S-parameters according to the equivalent medium theory [20]. In Fig. 7(b), the refractive index of the AML remains stable over the operating frequency band and is similar to the refractive index of air, which enables the AML to operate over a wide bandwidth. In (c) and (d) of Fig. 7, we can see that impedance, relative permittivity and permeability are close to 1, which approaches to air. This can provide a good impedance matching between the AML and air.

AML is not only required to have a transmission effect on electromagnetic waves, but also to have a focusing effect on electromagnetic waves. We use the law of refraction to simply analyze the focusing effect of electromagnetic waves in the antenna aperture, as shown in Fig. 8. In this figure, $n_1$is the effective refractive index of AML, and n_0 is the refractive index of air. According to the law of refraction, i.e. $n_1 \sin\alpha_1 = n_0 \sin\alpha_0$, there is a larger refractive angle (α_0) when n_1 is larger than n_0. It means that light is focused when it is incident from a medium with a large refractive index to a medium with a small refractive index. The electromagnetic wave in the antenna aperture is focused when passing through AML, so the directivity of the antenna is improved and the gain is enhanced.

On the other side, the SSR enhances the gain by reflecting electromagnetic waves. Simulated reflection and transmission coefficients are shown in Fig.9. It can be found that the magnitude of reflection coefficients (|S11|) from 1.0 GHz to 1.4 GHz are more than -10 dB. This means that when the electromagnetic wave passes through the SSR, most of the energy is reflected back. Electromagnetic waves of different frequencies are incident on the SSR at different incident angles. When the reflected electromagnetic waves are superimposed in the antenna aperture, the gain of the antenna gets enhanced. A simple optical path diagram of the SSR acting on the electromagnetic waves can be seen in Fig.8.

In order to reveal the influence of AMs on the antenna in different frequency bands more intuitively, the simulated electric field distribution is shown in Fig. 10. We still choose 0.7 GHz, 1.4 GHz and 2.1 GHz as the reference frequency points. By comparing the original antenna with the proposed electric field distribution of the antenna, it can be seen that the effect of the two artificial materials on the antenna is different at different frequency points. With increase of the

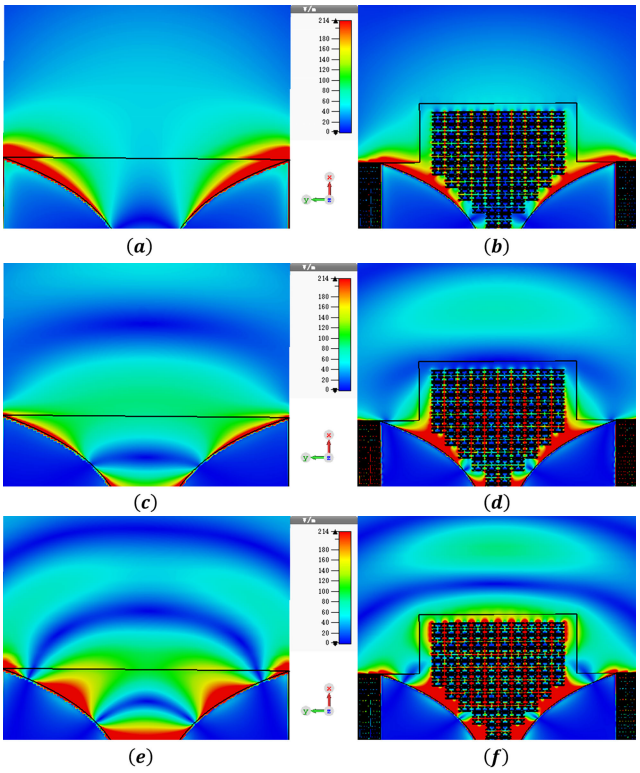

FIGURE 10. Simulated electric field distribution of CVAs. Without AMs: (a) 0.7 GHz, (c) 1.4 GHz, (e) 2.1 GHz. With AMs: (b) 0.7 GHz, (d) 1.4 GHz, (f) 2.1 GHz.

energy distribution of the electric field slowly shifts from the SSR to the AML. This shows that SSR mainly acts on low frequency electromagnetic waves and AML mainly acts on high frequency electromagnetic waves.

IV. CONCLUSION

AML and SSR are designed to enhance the gain of different frequency bands of the antenna without affecting other antenna performance. On the one hand, the AML acts as a lens to focus the electromagnetic waves by means of transmission. On the other hand, the SSR acts as a sidelobe suppressor to focus the electromagnetic waves by means of reflection. AML mainly acts on high-frequency electromagnetic waves, and SSR mainly acts on low-frequency electromagnetic waves. The combination of two kinds of artificial materials provides a new idea to improve the antenna's gain at low frequency operating band. The proposed antenna can be widely used in bottoming radar and wireless communication owing to its simple structure, low manufacturing cost, and excellent performance.

REFERENCES

[1] M. Moosazadeh, S. Kharkovsky, J. T. Case, and B. Samali, "Improved radiation characteristics of small antipodal vivaldi antenna for microwave and millimeter-wave imaging applications," *IEEE Antennas Wireless Propag. Lett.*, vol. 16, pp. 1961–1964, 2017.

[2] F. Zhang, G.-Y. Fang, Y.-C. Ji, H.-J. Ju, and J.-j. Shao, "A novel compact double exponentially tapered slot antenna (DETSA) for GPR applications," *IEEE Antennas Wireless Propag. Lett.*, vol. 10, pp. 195–198, 2011.

[3] L. Guo, H. Yang, Q. Zhang, and M. Deng, "A compact antipodal tapered slot antenna with artificial material lens and reflector for GPR applications," *IEEE Access*, vol. 6, pp. 44244–44251, 2018.

[4] K. Kim, W. R. Scott, and S. Member, "Design of a Resistively loaded Vee dipole for radar applications," *IEEE Trans. Antennas Propag.*, vol. 53, no. 8, pp. 2525–2532, Aug. 2005.

[5] M. Serhir and D. Lesselier, "Wideband reflector-backed folded bowtie antenna for ground penetrating radar," *IEEE Trans. Antennas Propag.*, vol. 66, no. 3, pp. 1056–1063, Mar. 2018.

[6] L. Guo, B. Xiao, M. Li, H. Yang, and H. Lin, "A high-gain and frequency-tunable bow tie antenna with epsilon-negative metasurface," *J. Electromagn. Waves Appl.*, vol. 29, no. 5, pp. 693–702, Mar. 2015.

[7] L. Sang, X. Li, T. Chen, and G. Lv, "Analysis and design of tapered slot antenna with high gain for ultra-wideband based on optimisation of the metamaterial unit layout," *IET Microw., Antennas Propag.*, vol. 11, no. 6, pp. 907–914, May 2017.

[8] A. Z. Hood, T. Karacolak, and E. Topsakal, "A small antipodal vivaldi antenna for ultrawide-band applications," *IEEE Antennas Wireless Propag. Lett.*, vol. 7, pp. 656–660, 2008.

[9] E. W. Reid, L. Ortiz-Balbuena, A. Ghadiri, and K. Moez, "A 324-element vivaldi antenna array for radio astronomy instrumentation," *IEEE Trans. Instrum. Meas.*, vol. 61, no. 1, pp. 241–250, Jan. 2012.

[10] A. M. De Oliveira, M. B. Perotoni, S. T. Kofuji, and J. F. Justo, "A palm tree antipodal vivaldi antenna with exponential slot edge for improved radiation pattern," *IEEE Antennas Wireless Propag. Lett.*, vol. 14, pp. 1334–1337, 2015.

[11] G. Teni, N. Zhang, J. Qiu, and P. Zhang, "Research on a novel miniaturized antipodal Vivaldi," *IEEE IEEE Antennas Wireless Propag. Lett.*, vol. 12, pp. 417–420, 2013.

[12] J. Bourqui, M. Okoniewski, and E. C. Fear, "Balanced antipodal vivaldi antenna with dielectric director for near-field microwave imaging," *IEEE Trans. Antennas Propag.*, vol. 58, no. 7, pp. 2318–2326, Jul. 2010.

[13] B. Zhou and T. J. Cui, "Directivity enhancement to vivaldi antennas using compactly anisotropic zero-index metamaterials," *IEEE Antennas Wireless Propag. Lett.*, vol. 10, pp. 326–329, 2011.

[14] S. Kundu, A. Chatterjee, S. K. Jana, and S. K. Parui, "A compact umbrella-shaped UWB antenna with gain augmentation using frequency selective surface," *Radioengineering*, vol. 27, no. 2, pp. 448–454, Jun. 2018.

[15] E. Erfani, M. Niroo-jazi, and S. Tatu, "A high-gain broadband gradient efractive index metasurface lens antenna," *IEEE Trans. Antennas Propag.*, vol. 64, no. 5, pp. 1968–1973, May 2016.

[16] A. R. H. Alhawari, A. Ismail, M. A. Mahdi, and R. S. A. R. Abdullah, "Antipodal Vivaldi antenna performance booster exploiting snug-in negative index metamaterial," *Prog. Electromagn. Res. C*, vol. 27, pp. 265–279, 2012.

[17] Y. Tsuji, Y. Morita, and K. Hirayama, "Photonic crystal waveguide based on 2-D photonic crystal with absolute photonic band gap," *IEEE Photon. Technol. Lett.*, vol. 18, no. 22, pp. 2410–2412, Nov. 2006.

[18] L. Chen, Z. Lei, R. Yang, J. Fan, and X. Shi, "Patch antenna to improve the radiation ef fi ciency. A low-loss LWG A Broa dBand Arti fi cial material for gain enhancement of antipodal tapered slot antenna," *IEEE Trans. Antennas Propag.*, vol. 63, no. 1, pp. 395–400, Jan. 2015.

[19] X. Li, H. Zhou, Z. Gao, H. Wang, and G. Lv, "Metamaterial slabs covered UWB antipodal vivaldi antenna," *IEEE Antennas Wireless Propag. Lett.*, vol. 16, pp. 2943–2946, 2017.

[20] D. R. Smith, D. C. Vier, T. Koschny, and C. M. Soukoulis, "Electromagnetic parameter retrieval from inhomogeneous metamaterials," *Phys. Rev. E, Stat. Phys. Plasmas Fluids Relat. Interdiscip. Top.*, vol. 71, no. 3, pp. 1–11, Mar. 2005.

[21] M. Amiri, A. Ghafoorzadeh-Yazdi, and A.-A. Heidari, "Gain and lower cut-off frequency improvement of antipodal vivaldi antenna," in *Proc. 8th Int. Symp. Telecommun. (IST)*, Sep. 2016, pp. 386–390.

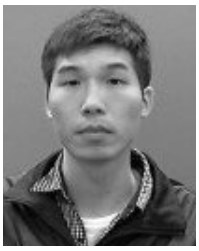

HOUYUAN CHENG is currently pursuing the master's degree with the Department of Information and Communication Engineering, Central China Normal University, Wuhan, China, focusing on the applications of metamaterials in antennas.

HELIN YANG received the M.S. degree in radio physics from Wuhan University, Wuhan, China, in 1996, and the Ph.D. degree in radio physics from Central China Normal University, Wuhan, in 2005. He joined the Department of Physics, Hexi University, Zhangye, China, as a Lecturer, in 1985, where he was promoted to an Associate Professor, in 1998. Since 1999, he has been with Central China Normal University, Wuhan, where he is currently a full-time Professor with the College of Physical Science and Technology. He has authored or coauthored more than 100 papers in refereed journals and conference proceedings. His current research interests include computational electromagnetics, electromagnetic compatibility, and microwave metamaterials.

YUJUN LI is currently pursuing the master's degree with the Department of Electronic Circuit and System, Central China Normal University, Wuhan, China, focusing on the applications of metamaterials in absorption and antennas.

YIQUN CHEN was born in 1981. He received the M.S. degree in geophysics and petroleum resources from Yangtze University, Jingzhou, China, engaged in teaching and research of engineering seismic exploration. He is currently a Lecturer with Yangtze University.